water

MDPI

Article

Geochemical Characteristics and Genesis of Brine Chemical Composition in Cambrian Carbonate-Dominated Succession in the Northeastern Region of Chongqing, Southwestern China

Zhi-lin Zheng [1], Bin Xie [1], Chun-mei Wu [1], Lei Zhou [1], Ke Zhang [2], Bin-chen Zhang [3] and Ping-heng Yang [4,*]

[1] No. 208 Hydrogeological and Engineering Geological Team, Chongqing Bureau of Geological and Mineral Resource Exploration and Development, Chongqing 400711, China; 15923347226@163.com (Z.-l.Z.); xiebin106256@163.com (B.X.); 18602310430@163.com (C.-m.W.); 13657677378@163.com (L.Z.)
[2] College of Humanities and Development Studies, Beijing 100091, China; kecorrine94chaie@163.com
[3] Chongqing Institute of Geological Survey, Chongqing 401121, China; 13629792756@163.com
[4] Chongqing Jinfo Mountain Karst Ecosystem National Observation and Research Station, School of Geographical Sciences, Southwest University, Chongqing 400715, China
* Correspondence: balance@swu.edu.cn

Abstract: Deeply situated brine is abundant in rare metal minerals, possessing significant economic worth. To the authors' knowledge, brine present within the Cambrian carbonate-dominated succession in the northeastern region of Chongqing, Southwestern China, has not been previously reported. In this investigation, brine samples were collected from an abandoned brine well, designated as Tianyi Well, for the purpose of analyzing the hydrochemical characteristics and geochemical evolution of the brine. Halide concentrations, associated ions, and their ionic ratios within the sampled brine were analyzed. The brine originating from the deep Cambrian aquifer was characterized by high salinity levels, with an average TDS value of 242 ± 11 g/L, and was dominated by a Na-Cl facies. The studied brine underwent a moderate degree of seawater evaporation, occurring between the saturation levels of gypsum and halite, accompanied by some halite dissolution. Compared to modern seawater evaporation, the depletion of Mg^{2+}, HCO_3^-, and SO_4^{2-} concentrations, along with the enrichment of Ca^{2+}, Li^+, K^+, and Sr^{2+}, is likely primarily attributed to water–rock interactions. These interactions include dolomitization, combination of halite dissolution, upwelling of lithium- and potassium-bearing groundwater, calcium sulfate precipitation, biological sulfate reduction (BSR), and the common ion effect within the brine system. This research offers valuable insights into the genesis of the brine within the Cambrian carbonate succession and provides theoretical backing for the development of brine resources in the future.

Keywords: brine; genesis; chemical composition; water–rock interactions; Cambrian carbonate

Citation: Zheng, Z.-l.; Xie, B.; Wu, C.-m.; Zhou, L.; Zhang, K.; Zhang, B.-c.; Yang, P.-h. Geochemical Characteristics and Genesis of Brine Chemical Composition in Cambrian Carbonate-Dominated Succession in the Northeastern Region of Chongqing, Southwestern China. *Water* **2024**, *16*, 2859. https://doi.org/10.3390/w16192859

Academic Editor: Pankaj Kumar

Received: 8 August 2024
Revised: 1 October 2024
Accepted: 3 October 2024
Published: 9 October 2024

1. Introduction

The deeply buried regions within most sedimentary basins contain substantial volumes of brines [1–4], which exert pivotal influences on diverse geological processes—including natural resource development—while holding significant implications for both scientific research and economic utilization [5]. The basinal brines (also referred to as formation waters or oil-field saline solutions) typically exhibit salinity levels ranging from 10 to 300 g/L [6]. The majority of brines belong to either Na-Cl or Ca-Cl facies, distinguished chemically by their elevated concentrations of Ca^{2+}, surpassing combined levels of SO_4^{2-}, HCO_3^-, and CO_3^{2-} ions compared to seawater and other common surface/near-surface water types (e.g., Na-Cl-SO_4 or Ca-HCO_3 facies). Evaporite deposits found within the basins commonly originated from the evaporation of isolated seawater [7]. The brines are either connate ones that have persisted since the early Paleozoic era—which have been trapped since the early Paleozoic era in these closed basins with restricted groundwater circulation [8,9]—or brines

that have emerged from the dissolution of the evaporite deposits themselves [10,11]. The chemical compositions of brines offer valuable insights into geochemical, hydrological, and tectonic developments within the Earth's crust as well as providing an understanding of several pertinent issues relating specifically to metal ore deposits, dolomitized reservoirs, and hydrocarbon exploration/production [12,13]. Notably, dissolved metals tend to be prevalent within saline solutions exceeding 200 g/L [6].

The sedimentary brines present themselves as exceptional natural phenomena shrouded in unresolved enigmas concerning their origin and evolution of chemical compositions. Genesis behind the brines poses an essential and captivating challenge within contemporary hydrogeological/hydrogeochemical communities [14]. Potential hypotheses regarding the genesis of brine chemical compositions include evaporite dissolution, subaerial seawater evaporation, interactions between rocks and water, osmotic/membrane filtration, and ion exchanges [9,15–20]. The divergent viewpoints on the genesis of brine arise not only from their unique chemical compositions and extreme salinity but also from their extensive distribution across various continental crustal blocks on Earth.

The chemistry of groundwater is significantly influenced by the mineralogical composition of the aquifer it traverses. The chemistry of major ions and their interrelationships in groundwater are effective in identifying the origins of solutes and elucidating the evolution of groundwater [21]. The chemical composition reflects the evolution of groundwater and serves as a crucial method for investigating the formation of brines. This includes the application of ion ratio methods such as Cl^-/Br^- [22–24], Ca excess and Na deficit relative to modern seawater reference ratios [25], and comparison of cation and anion abundances in brines with modern seawater [26]. Significant advancements have been achieved in understanding the genesis of brine composition through hydrochemical studies [5,12,13,27,28].

To the authors' knowledge, Cambrian-era sedimentary brine occurrences remain unreported in the region of the northeastern Chongqing municipality, Southwestern China. Such occurrences are part of this enigma since questions about their genesis remain unresolved. This study aims to investigate the hydrochemical characterization of brine in northeastern Chongqing to understand its geochemical evolution by utilizing the halide concentrations and associated ions from an abandoned brine well, Tianyi Well. This reconnaissance hyrdogeochemical study may provide valuable insights into economic explorations within deep geological environments in the study area.

2. Description of the Area Adjacent to the Studied Brine

2.1. Location and Geographical Settings

The study area is located in Wuxi County, positioned in northeastern Chongqing, SW China (Figure 1a–c). It is characterized by mountainous terrain with significant relief, ranging from 320 to 1790 m above sea level.

It is within a subtropical monsoon climate, with an average annual temperature of 18 °C. In January, the average temperature is 8 °C, while in July it rises to 35 °C. The region receives an average annual precipitation of 1450 mm, concentrated mainly between May and October each year, peaking in September.

2.2. Geological Settings

Apart from the absence of Devonian and Carboniferous strata due to geological denudation, the exposed formations adjacent to the studied Tianyi Well range from the Cambrian to Triassic (Figure 1d). The Triassic strata consist mainly of limestone, with minor occurrences of dolomitic limestone and gray-to-gray-purple calcareous shale, reaching an overall thickness exceeding 350 m. The Permian strata are predominantly composed of limestone, accompanied by iron clay and coal seams, with a total thickness ranging from 510 to 931 m. The Silurian strata are characterized by quartz sandstone, mudstone, and shale, measuring between 852 and 1053 m in thickness. The Ordovician strata primarily comprises limestone, dolomite, argillaceous dolomite, and silty shale, with an aggregate

thickness of 304–391 m. The Cambrian strata are chiefly composed of dolomite interbedded with evaporites, with a total thickness surpassing 775 m. The region is mainly underlain by Archean deeply metamorphosed basic–ultrabasic metamorphic rocks [29].

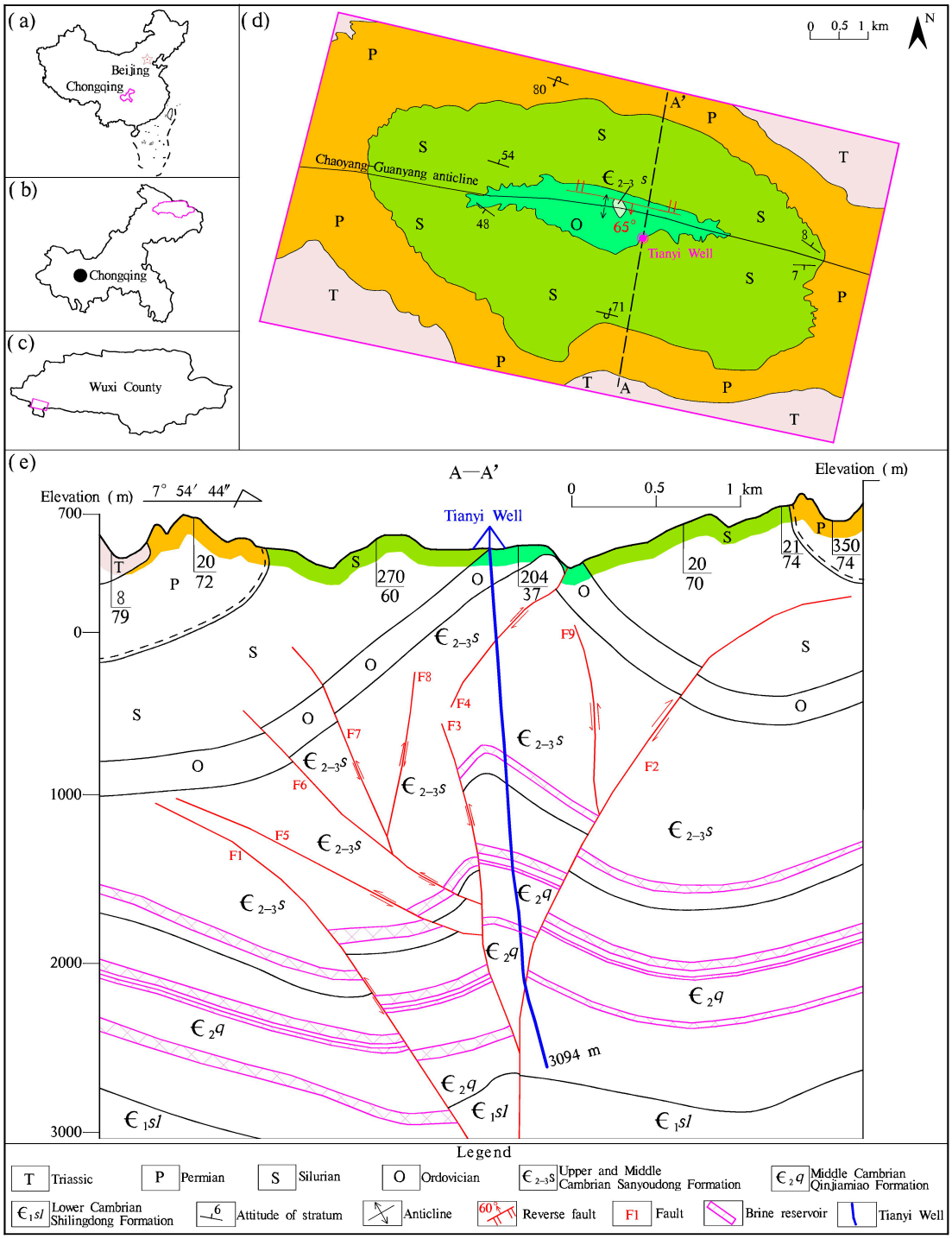

Figure 1. (**a**–**c**) Location of the studied brine of Tianyi Well, (**d**) its adjacent outcrops, and (**e**) cross-section A-A′ showing an overview of the general lithology of the well and surrounding successions, in which the faults were identified through seismic wave analysis.

The primary tectonics in this area is a steeply dipping reverse fault, measuring 1.7 km in length, which has developed within the paraxial part of the Chaoyang–Guanyang anticline extending northwestward (Figure 1d). This fault exhibits a dip angle of 50–70°

and a dip direction at approximately 190°. The upper hanging wall consists of Middle and Upper Cambrian Sanyoudong Formation ($\in_{2-3}$s) carbonate, displaying distinct features of thrusting and extrusion, whereas the footwall comprises shale of the Ordovician Formation. The fracture bandwidth measures between 2 and 5 m with landforms aligning along its trend for about the maximum distance. Additionally, seismic wave analysis indicates the significant presence of regional underground reverse faults (Figure 1e), which may restrict fluid movement in the vicinity. The Tianyi Well—the building of which commenced in 1964—was drilled to a depth of 3094 m along the anticlinal axis, traversing through the Upper and Middle Cambrian Sanyoudong Formation ($\in_{2-3}$s) as well as the Middle Cambrian Qinjiamiao Formation ($\in_2$q) (Figure 1e).

The strata closely associated with brine primarily belong to the Cambrian succession. The following provides a lithological overview of the Upper and Middle Cambrian Sanyoudong Formation ($\in_{2-3}$s) and Middle Cambrian Qinjiamiao Formation ($\in_2$q).

Sanyoudong Formation ($\in_{2-3}$s): The upper portion of this formation consists of gray-to-dark-gray medium-thick bedded dolomite interbedded with gray-yellow medium-thick bedded breccia dolomite, and some bioclastic limestone. Horizontal bedding prevails occasionally accompanied by sutures and mold structures. The thickness of the formation ranges from 235.1 to 297 m in the area; however, drilling at Tianyi Well encountered a fault resulting in repeated formation with a drilling thickness of 1173.5 m and a true vertical thickness of 4277 m (Figure 1e). At the lower end lies a thick-bedded dolomitic medium-grained quartz sandstone layer with an approximate thickness of 2 m. Based on Tianyi Well's drilling data, the underground brine reservoir was discovered between depths of 1239 and 1278 m below the wellhead (Figure 1e).

Qinjiamiao Formation ($\in_2$q): This formation remains unexposed on the regional surface but the drilling core indicates predominantly thin-layer argillaceous dolomite alongside light gray and yellow-gray thin-to-medium-layer sandy dolomite embedded with dolomite, gypsum, and salt soluble breccia. Drilling at Tianyi Well reached depths of 1752 m with a true vertical thickness of 385.2 m. This formation yielded three brine reservoirs, located at depths of 1790–1839, 1895.4–1912.0, and 2250.4–2288.7 m, respectively, below the wellhead (Figure 1e). The porosity of the brine reservoirs ranges from 1.0 to 24.0%, with a weighted average porosity of 2.0%.

From a stratigraphic perspective, during the epoch spanning the Middle- and Upper-Cambrian periods, a considerable regression in seawater occurred in a hot climate, which facilitated the development of lagoon-like sedimentary facies on confined platforms. Following this, the intensified evaporation process led to the emergence of Sabkha environments, conducive to the substantial deposition of salt minerals. Specifically, the carbonates were initially deposited in shallow waters, likely in tidal flat or lagoonal environments. As evaporation continued to intensify, gypsum and halite successively precipitated and deposited. However, at Tianyi Well, a clean water drilling technique was utilized below a depth of 340 m under the wellhead, thereby impeding the acquisition of rock cores essential for confirming the existence of halite layers within the Sanyoudong and Qinjiamiao Formations. Approximately 150 km from this location, a drilled well struck a layer of halite deposit measuring 120 m in thickness within the Cambrian carbonate strata beneath the surface [30]. This confirmed the presence of salt minerals in the area.

From a hydrogeological perspective, the deep-seated structural faults in this region are predominantly reverse faults (Figure 1e), formed under compressive stress conditions. As these faults evolved, the rocks along the fault plane and within the fault zone underwent significant compression, resulting in the formation of dense rock strata that serve as a barrier to shield the underlying brine. However, it is possible for rainwater to infiltrate into the subterranean realm via the exposed Ordovician carbonates, as depicted in Figure 1e. This infiltration process may exert a discernible dissolving influence upon the brine, potentially altering its composition.

3. Methodology and Materials

3.1. Field Sampling

Brine samples were collected at the surface from the Tianyi Well by pumping. The pumping operation was conducted within the timeframe of 23–28 November 2023, wherein the brine was extracted from a depth of 1008 m beneath the surface of the wellhead, and the entire process lasted for a duration of 66 h. The pumping discharge ranged from 0 to 13 m^3/h and it stabilized at approximately 11 m^3/h. Upon cessation of pumping, the recovery period of the water level took 47.9 h (Figure 2). The extracted brine was the result of the mixture of the entire well, representing the overall condition of the deep brine system. The pumped brine, characterized by its gray-black coloration, was translucent yet cloudy, bearing a saline character with suspended particles. It also released a rotten egg smell, which is from hydrogen sulfide (H_2S) gas. The brine samples were collected in strict adherence to protocol after being pumped to the surface. During the pumping activity, one brine sample was collected every 2 h within the first 6 h of pumping, followed by samples collected every 4 h (Figure 2). A total of 19 brine samples were obtained. High-density poly ethylene bottles, 5 L in size, were used for brine sample collection. To prevent contamination, sampling bottles were rinsed with the sampled brine five times prior to collection. All brine samples were immediately stored in a cool and sealed environment after sampling, and then transported back to the laboratory within 24 h for measurement.

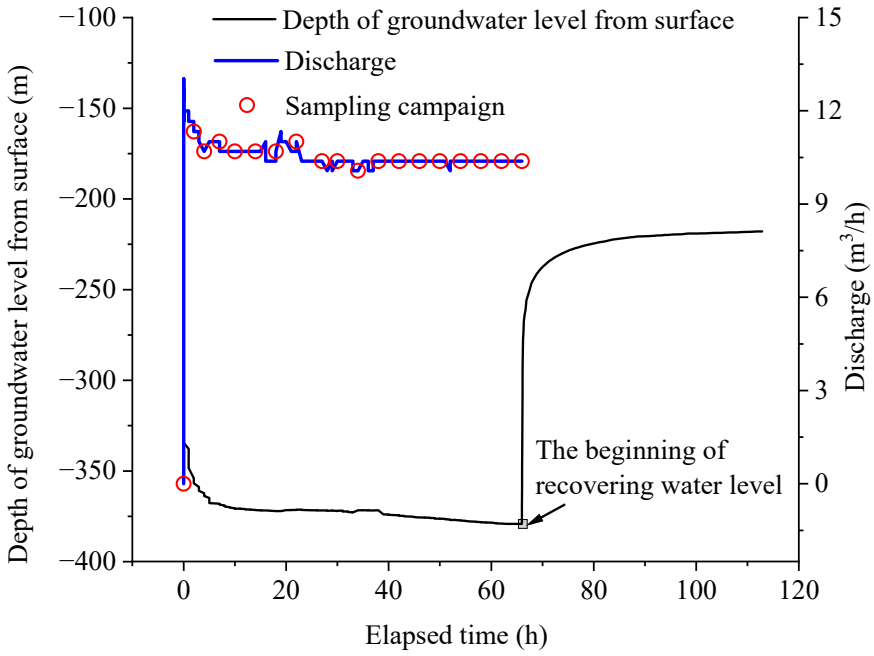

Figure 2. Pumping, recovering water level, and sampling campaign of the studied brine.

3.2. Measurement

Na^+, K^+, Ca^{2+}, Mg^{2+}, Li^+, SO_4^{2-} concentrations were analyzed using an ICP-OES Avio 200 (PerkinElmer Company, Waltham, MA, USA). Cl^- and HCO_3^- concentrations were determined using brown and white acid burettes, respectively. Br^- concentration was measured using an Ultraviolet spectrophotometer UV2700 (Shimadzu Corporation, Kyoto, Japan). The accuracy of ion concentration testing is better than 0.01 mg/L. The measurements were carried out at the Salt Lake Chemical Analysis Test Center of Qinghai Institute of Salt Lake Research, Chinese Academy of Sciences, under laboratory conditions with a temperature of 20 °C and relative humidity of 29%.

4. Result and Discussion

4.1. Hydrochemistry

The main concentrations of cations and anions in the studied brine from the Tianyi Well are listed in Table 1. From the dynamic variations in TDS and ion concentration during the pumping process, the TDS value of the studied brine increased from 211 to 247 g/L within 10 h of the initial pumping, and then stabilized at ~246 g/L during the subsequent pumping process (Figure 3). This stabilization of the TDS values suggests a relatively closed brine aquifer. However, the average TDS value of 242 ± 11 g/L significantly exceeds that of modern seawater with a value of 3.3 g/L, and the geothermal water at a circulation depth of 1.3 km around the study area within 100 km exhibiting concentrations ranging from 57.6 to 88.7 g/L [31]. The pattern of total milliequivalents of cations and anions, and concentrations for cations and anions in brine were similar to TDS, which increased within 10 h at the beginning of pumping and then stabilized in the region (Table 1; Figure S1).

Table 1. Physical and chemical parameters of the studied brine.

Elapsed Time	K^+	Na^+	Ca^{2+}	Mg^{2+}	Li^+	Sr^{2+}	Br^-	CO_3^{2-}	HCO_3	Cl^-	SO_4^{2-}	pH	TDS	Na^+: Cl^-	TMMC	TMMA	Balance Test
0	2992	72,159	6562	1028	89	226	357	78.09	154	128,196	1223	7.88	211	0.87	3650	3631	0.25
2	2645	73,010	5657	972	79	183	279	20.13	196	124,732	4780	7.70	210	0.90	3625	3571	0.75
4	3410	82,816	7243	1205	101	249	384	<0.43	148	146,290	1905	7.33	241	0.87	4175	4149	0.32
6	3366	81,077	7027	1195	99	244	354	<0.43	66	142,966	2147	7.33	236	0.87	4086	4056	0.37
10	3500	85,051	7186	1244	103	249	402	<0.43	150	149,126	2875	7.08	247	0.88	4275	4238	0.44
14	3455	84,655	7380	1243	103	247	375	<0.43	150	148,864	2808	7.10	247	0.88	4266	4230	0.43
18	3533	84,726	7252	1264	101	246	364	<0.43	151	148,963	2675	7.02	247	0.88	4266	4232	0.41
22	3481	83,501	7113	1241	101	243	363	<0.43	152	146,152	3440	7.03	245	0.88	4203	4160	0.51
26	3523	84,664	7404	1298	104	253	382	<0.43	153	148,574	3584	7.05	249	0.88	4275	4230	0.51
30	3571	83,368	7228	1255	103	250	387	<0.43	156	146,176	3587	7.28	247	0.88	4207	4163	0.53
34	3573	83,425	7215	1285	102	249	371	<0.43	152	146,631	3167	7.33	247	0.88	4211	4171	0.47
38	3475	82,861	7047	1266	102	249	363	<0.43	156	145,470	2965	7.34	243	0.88	4174	4136	0.45
42	3532	84,076	7153	1257	102	246	358	<0.43	164	146,211	4789	7.31	249	0.89	4233	4176	0.67
46	3507	83,765	7252	1272	101	249	364	<0.43	153	146,754	3663	7.28	247	0.88	4225	4180	0.53
50	3470	83,340	7092	1278	102	249	391	<0.43	152	145,950	3465	7.33	244	0.88	4198	4155	0.52
54	3531	84,822	7166	1251	103	244	383	<0.43	149	148,133	3752	7.30	249	0.88	4265	4219	0.54
58	3567	83,197	7157	1279	103	247	370	<0.43	152	146,173	3154	7.27	246	0.88	4198	4158	0.47
62	3508	84,283	7054	1245	103	246	397	<0.43	156	147,365	3351	7.27	247	0.88	4236	4194	0.50
66	3535	84,153	7270	1260	103	246	395	<0.43	156	147,021	4152	7.34	248	0.88	4243	4192	0.60
	3430 *	825,76 *	7077 *	1228 *	100 *	243 *	370 *		151 *	144,724 *	3236 *	7.29 *	242 *	0.88 *	4158 *	4118 *	

Note: elapsed time is in h; the concentrations of major ions are in mg/L; TDS is in g/L; Na^+: Cl^- is in molar ratio; TMMC and TMMA stand for the total milliequivalent of major cations, total milliequivalent of major anions, respectively; balance test is in %; * is denoted as average value.

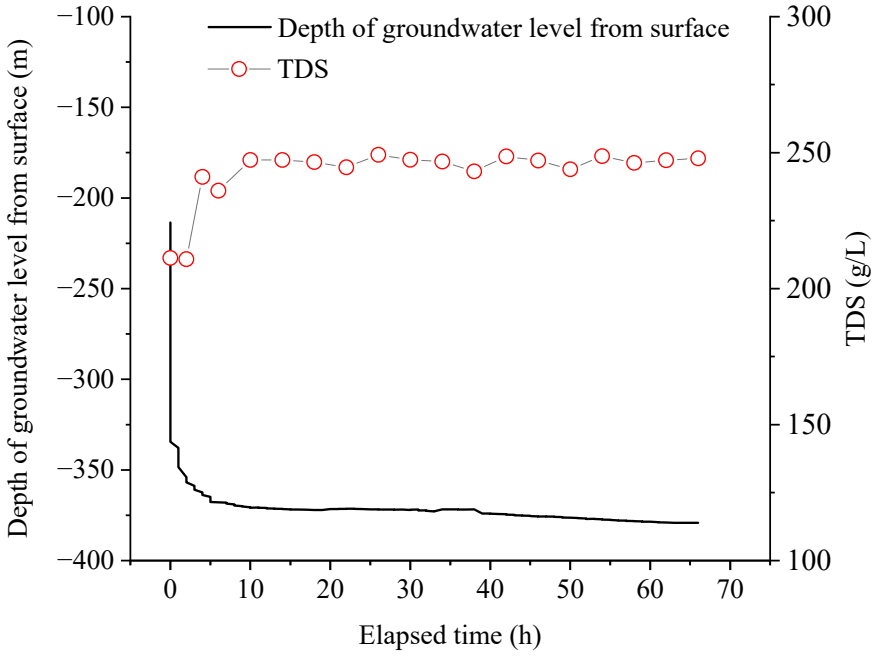

Figure 3. Variation in TDS values during pumping.

From the perspective of mean concentration, the milliequivalent of major cations ($Na^+ + K + Ca^{2+} + Mg^{2+} + Sr^{2+} + Li^+$) in the studied brine was 4154 ± 184 mEq/L, while it

was 4118 ± 182 mEq/L for anions (Cl^- + SO_4^{2-} + HCO_3^-). The milliequivalent of major ions significantly exceeded that of geothermal water in both the northeastern region and the main urban area, ranging from 24.3 to 45.6 mEq/L for cations and from 24.3 to 47.6 mEq/L for anions [31,32]. The trends in anion and cation concentrations corresponded with the TDS levels, maintaining a relatively stable state (Table 1; Figure S1). It is noteworthy to mention that the presence of potassium (averaging at 3430 ± 223 mg/L), lithium (averaging at 100 ± 6 mg/L), and bromine (averaging at 370 ± 26 mg/L) in brine possesses significant industrial mining potential. However, the economic exploitation of these ions does not constitute the primary objective of this study, and therefore, will not be further discussed.

The hydrochemical facies serves as a fundamental method for conducting hydrogeochemical and environmental geochemical investigation, providing crucial insights into the characteristics of groundwater's chemical components. Currently, the Piper trilinear diagram introduced by Piper in 1944 as a renowned graphical tool for water chemistry analysis [33] has been predominantly employed to investigate hydrochemical facies. The diagram has been extensively utilized within the field of hydrochemistry [34–37]. By projecting the chemical component data of the studied brine samples onto the Piper trilinear diagram as shown in Figure 4, it can be observed that the dominant hydrochemical facies of the studied brine is Na-Cl. The studied brine, comprising of Na-Cl facies and having an average TDS value of 242 ± 11 g/L, falls within the range of chloride-dominated, halite-undersaturated waters as outlined by Hanor (1994) [6]. This range varies between 10 g/L and the upper threshold of 250–300 g/L [6].

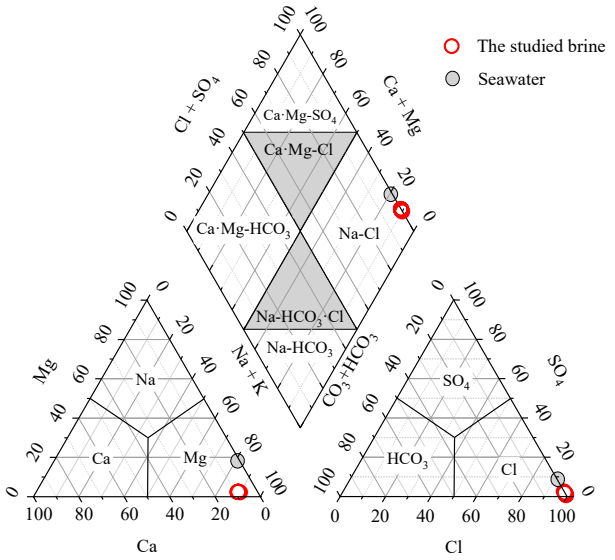

Figure 4. Piper trilinear diagram shows that the studied brine was a Na-Cl hydrochemical facies.

In 1970, Gibbs [38] introduced a graphical method to identify the sources of the main chemical elements in water bodies. This diagram categorizes the main formation mechanisms of water chemical components into three categories: atmospheric precipitation, rock weathering dominance, and evaporation–crystallization process. The method primarily utilizes the relationship between the TDS value and (K^+ + Na^+)/(K^+ + Na^+ + Ca^{2+}) as well as Cl^-/(Cl^+ + HCO_3^-) in the mEq/L ratio. Although initially proposed for surface water chemistry research [38,39], Gibbs's diagram has been widely adopted in groundwater research [40–43]. All the studied brine samples were positioned within the realm of the evaporation–crystallization process (Figure 5). This observation together with the extremely high TDS values indicates that the brine originated from evaporated ancient seawater.

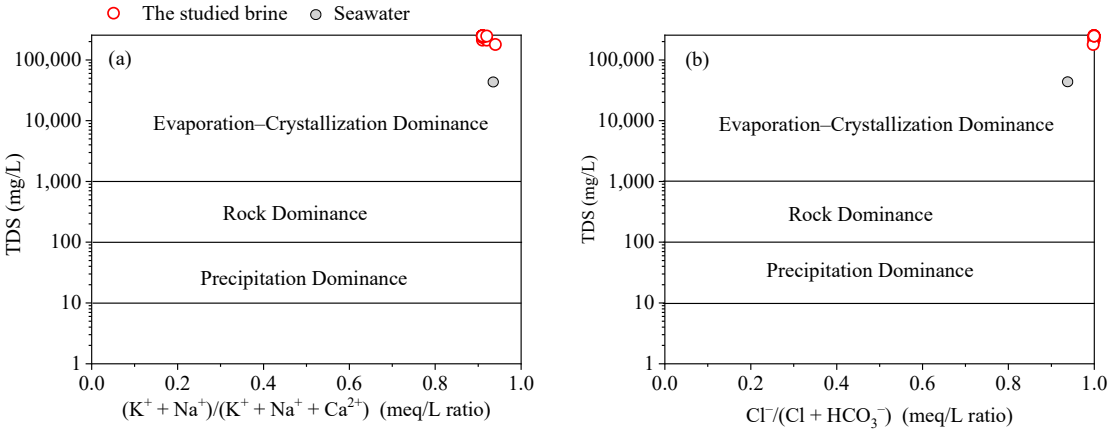

Figure 5. Gibbs's diagram depicts the range of brine studied, falling within the evaporation–crystallization process. The plot was adapted from Gibbs (1970) [38].

4.2. Stages of Brine Evolution

Chloride and bromine are halogen elements found in most groundwater. Cl^- and Br^- emerge as ideal indicators for studying the chemical evolution of brines due to their relatively inert and conservative characteristics [22,23]. Cl^- and Br^- concentrations were widely used as indicators of evaporation and halogen dissolution in formation waters (Carpenter, 1978) [19]. The Cl^-/Br^- ratio maintains its stability during the evaporation of seawater, reaching a halt at the point of halite saturation (Figure 6). After this saturation, Cl^- is preferentially eliminated via halite precipitation, resulting in a decrease in the Cl^-/Br^- ratio, as Carpenter (1978) [19] observed. Conversely, during halite dissolution, the Cl^-/Br^- ratio rises, shifting the data points to the right of the seawater evaporation trajectory. When a brine, evaporated beyond the halite saturation point, is diluted by meteoric water, the mixture shifts to the left of the seawater evaporation trajectory (Figure 6). Based on this understanding, the data of the study area plot to the right of the seawater evaporation trajectory, situated between the points of gypsum and halite saturation (Figure 6). This suggests that the studied brine underwent a moderate level of seawater evaporation, specifically taking place at a phase when the brine's saturation point lay somewhere between the saturation levels of gypsum and halite, together with some extent of halite dissolution.

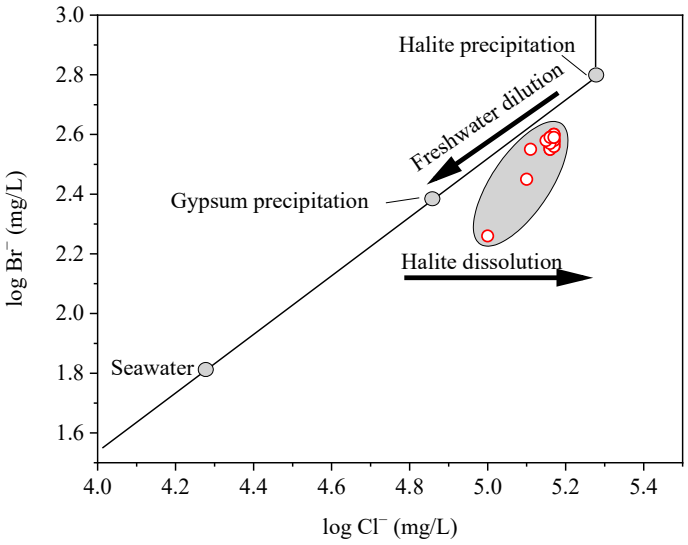

Figure 6. Cl^- vs. Br^- concentrations suggests a moderate level of evaporation between gypsum and halite saturation and some degree of halite dissolution.

The molar ratio of Na^+ to Cl^- in halite upon dissolution is 1:1. Conversely, the average molar ratio recorded in our studied brine samples exhibited a slight deviation, measuring 0.88, marginally surpassing the 0.86 ratio observed in seawater and indicating a subtle trend toward the dissolution ratio. This observation suggests that the composition of the studied brine primarily results from the evaporation of ancient seawater, with only a minor contribution from the dissolution process. Furthermore, these findings corroborate the validity of insights derived from the aforementioned Cl^-/Br^- ratio analysis. Additionally, the Giggenbach triangle plot (Figure S2) clearly indicates that the studied brine was saturated, providing further evidence that the primary source of the studied brine was from evaporated seawater, with halite dissolution as a secondary factor.

4.3. Potential Mechanisms Underlying the Ionic Enrichment or Depletion

To evaluate the extent of enrichment or depletion relative to evaporated modern seawater, Mirnejad et al. (2011) [26] utilized the abundances of cations and anions present in the brines as a means of evaluation. In this method, the average Cl^- concentration of all studied brine samples (144,724 mg/L) was initially divided by the Cl^- concentration in seawater from the Huanghai Sea, China (17,530 mg/L [44]), yielding a concentration factor. This factor was then multiplied with the concentration of each ion in seawater to estimate the concentration of these ions in evaporated seawater. Finally, the mean concentrations of the ions of the studied brine were normalized to the evaporated seawater concentrations by dividing the concentration of each ion by the corresponding concentration in the previously calculated evaporated seawater. The abundances of these ions in the studied brine are presented in Figure 7. The concentrations of Ca^{2+}, Li^+, Sr^{2+}, and Na^+ in the studied brine—standardized with respect to the chlorinity of modern seawater—were observed to be higher than those in evaporated modern seawater characterized by a value of 1, whereas the concentrations of K^+, Mg^{2+}, Br^-, HCO_3^-, and SO_4^{2-} were significantly lower. The anomalous patterns observed in ion concentrations suggest with certainty that the genesis of the studied brine cannot be solely attributed to seawater evaporation and halite dissolution but also involves distinct patterns of geochemical process that modify the brine's chemical composition in the study area.

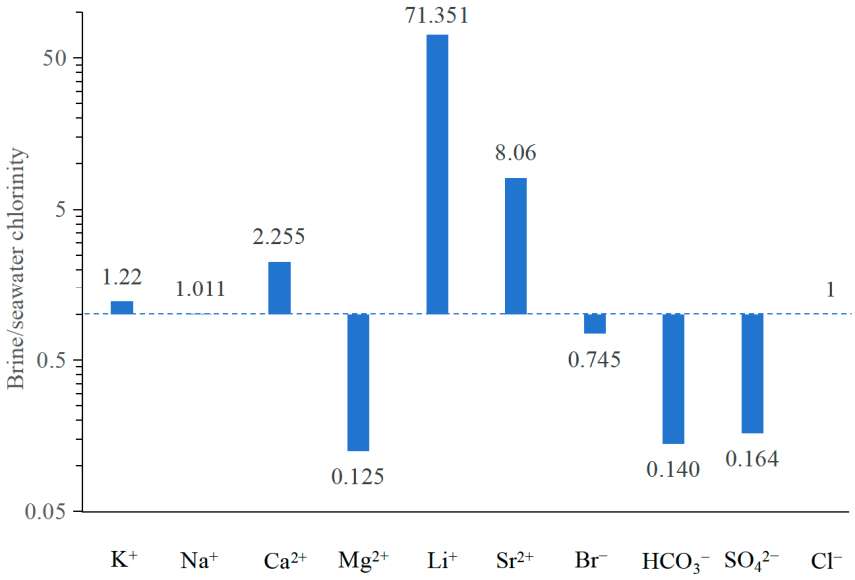

Figure 7. The ionic patterns of the studied brine standardized with respect to the chlorinity of modern seawater (concentrations from Chen, 1983), showing the brine cannot be attributed solely to the evaporation of seawater but also water–rock interactions. The value of dash line is 1 and indicates concentrated seawater. A value of 1 signifies equivalence to seawater, a value greater than 1 denotes an enrichment relative to seawater, whereas a value less than 1 indicates depletion compared to seawater.

The observed enrichment in Ca^{2+}, Li^{+}, K^{+}, Sr^{2+}, and Na^{+} concentrations and depletion in Mg^{2+}, Br^{-}, HCO_3^{-}, and SO_4^{2-} (Figure 7) is likely primarily attributable to the dolomitization process, combination of halite dissolution, upwelling of lithium- and potassium-bearing groundwater, calcium sulfate precipitation, biological sulfate reduction (BSR), and the common ion effect in the brine environments. This comprehension will be thoroughly examined and deliberated in the subsequent sections.

The Cambrian carbonate formations of the studied brine provide abundant $CaCO_3$ for dolomitization. The dolomitization involves the replacement of calcium carbonate (limestone) with calcium magnesium carbonate (dolomite), as expressed by Equation (1), thus resulting in a decrease in Mg^{2+} concentration and a dramatic increase in Ca^{2+} concentration that far exceeds the combined concentrations of SO_4^{2-} and HCO_3^{-}. The dolomitization ultimately made the studied brine calcium-rich. This phenomenon has been observed and documented in brines throughout the world, as evidenced by the studies conducted by Carpenter (1978) [22] and Gavrieli and Stein (2006) [45].

$$2CaCO_3 + Mg^{2+} = CaMg(CO_3)_2 + Ca^{2+} \quad (1)$$

The enrichment of Li^{+} concentration in the studied brine is likely due to a combination of halite dissolution and the influence of the crystalline basement. Although pegmatites and granites are the primary sources of Li^{+} [46], host rocks containing high-dissolved lithium brines are predominantly composed of carbonates, likely due to their inherently limited sorption capacities [27]. The lithium isotopic compositions (δ^7Li) of two brine samples were determined to be 12.58 and 12.8‰, respectively, significantly lower than the values observed in seawater (31‰ [47]). These measurements also fell below the range found in deep saline groundwater from the arid Atacama Desert region in Northern Chile, where values ranged between 23.5 and 31.5‰, suggesting a contribution from marine-derived salts and mineral alteration processes [48]. The δ^7Li values of the studied brine were much higher than those of deep-seated magmatic rocks in the region of western Sichuan, China (1.1‰ [49]). The lithium isotope values observed in the analyzed brine samples were situated between those of seawater and magmatic sources, suggesting that the Li^{+} likely originated from a combination of halite dissolution and the upwelling of lithium-bearing groundwater derived from alteration of minerals in the magmatic rocks within the region's crystalline basement. In a study conducted by Dugamin et al. [18], it was proposed that substantial enrichment of lithium occurs in brines that are primary in nature and initially in equilibrium with halite, and optimal reservoirs for lithium-rich brines are characterized by the accumulation of brine derived from evaporites during tectonic events, such as compressional events or salt tectonics, located in close proximity to the current reservoir. To maintain the integrity of these reservoirs and prevent dilution or depletion of lithium, it is crucial to shield them from convection and infiltration of surface water via recharge zones. Further investigation is warranted to elucidate the precise sources of these ions in the future utilizing lithium isotope technology.

The observed enrichment of K^{+} in the studied brine may align with the mechanism underlying Li^{+} enrichment. In addition to contributions from halite dissolution, it could also originated from the upwelling of potassium-rich fluids from the region's crystalline basement.

As indicated by Carpenter (1978) [22], the presence of Sr^{2+} in the brines exhibits a strong correlation with the recrystallization process of aragonite transforming into calcite. However, the Sr^{2+} ion possesses a radius comparable to that of Ca^{2+} and holds an identical valence, thereby facilitating its substitution for Ca^{2+} in the crystal lattices of diverse minerals, including kainite, plagioclase, gypsum, calcite, and dolomite [50]. Hence, the presence of Sr^{2+} in the studied brine is probably linked to the dolomitization process, which ultimately leads to the enrichment of Sr^{2+}.

The depletion of SO_4^{2-} in studied brine can be attributed to two primary mechanisms. Firstly, there is direct precipitation, where SO_4^{2-} combines with enriched Ca^{2+} to form calcium sulfate, which can manifest as either gypsum or anhydrite. This enrichment of Ca^{2+} is a direct consequence of the dolomitization process within the brine as previously

mentioned (Equation (1)), enhancing the availability of Ca^{2+} for precipitation reactions. This precipitation process is described by Equation (2):

$$Ca^{2+} + SO_4{}^{2-} = CaSO_4 \quad (2)$$

Secondly, sulfate reduction is another mechanism that contributes to the loss of $SO_4{}^{2-}$ from the brine. There are two types of sulfate reduction processes in the lithosphere [51]. The first type is biological sulfate reduction (BSR), which is mediated by microorganisms such as sulfate-reducing bacteria and occurs at relatively low temperatures, generally below 100 °C, and at depth of the strata less than 2000–2500 m. The second type is thermochemical sulfate reduction (TSR) involving hydrocarbons and sulfates, which typically takes place at temperatures exceeding 120 °C [51]. In this study of Tianyi Well, the water temperature at a depth of 1008 m was 45 °C, which suggests that BSR was the main process responsible for the $SO_4{}^{2-}$ depletion occurring there. A pronounced H_2S odor was detected from the brine during sampling, verifying the occurrence of BSR. The occurrence of sulfate reduction is convincingly demonstrated by the exceedingly low desulfurization coefficient (approaching a value of 0, Table S1) observed in the studied brine, thereby providing empirical support for the process. This BSR process, often accompanied by the precipitation of calcite, involves a complex set of reactions that reduce sulfate while producing a range of byproducts, including H_2S, water, CO_2, and ultimately, $CaCO_3$, as expressed by Equation (3). While the precise stoichiometry and intermediate steps of sulfate reduction may vary depending on specific conditions, a generalized representation of this process could be encapsulated by the following reaction scheme, as expressed in Equation (3) [22], with the understanding that the coefficients are illustrative and may not precisely reflect all scenarios.

$$Ca^{2+} + SO_4{}^{2-} + 1.33CH_2 = H_2S + CaCO_3 + 0.33H_2O + 0.33CO_2 \quad (3)$$

The depletion of $HCO_3{}^-$ concentration observed in the studied brine can be rationalized through the mechanism of the common ion effect. In carbonate aquifers, a high concentration of $HCO_3{}^-$ is expected; however, the brine in the study area exhibited a very low $HCO_3{}^-$ concentration averaging at 151 ± 22 mg/L (Table 1), even lower than that found in the karst shallow groundwater (~300 mg/L) located 400 km away from the Tianyi Well [52]. This substantial disparity may imply that $HCO_3{}^-$ in the studied brine precipitated with Ca^{2+} ions from the dissolution of gypsum/anhydrite within the geological formation to trigger calcite precipitation. This phenomenon, commonly referred to as the common ion effect, is frequently encountered in deep aquifers [32,53–55]. The chemical reaction governing this process can be expressed as follows:

$$2HCO_3{}^- + CaSO_4{\cdot}nH_2O \rightarrow CaCO_3 + CO_2 + SO_4{}^{2-} + (1 + n)H_2O \quad (4)$$

where n equals 2 for gypsum and 0 for anhydrite, highlighting the dissolution reactions specific to these minerals.

The mechanism of bromine depletion in brine in the studied brine is unclear. Theoretically, bromine is a highly stable element, and its concentration tends to remain nearly constant. It precipitates only when the evaporation rate reaches 90 times that of seawater [23]. However, the brine in this study was situated between gypsum saturation (3.8 times seawater [23]) and halite saturation (10.6 times seawater [23]) as aforementioned, indicating that the depletion of Br^- was likely influenced by additional factors. Further investigation is warranted.

The slight elevation in Na^+ concentration, as illustrated in Figure 7, suggests that the salinity of the brine has remained largely stable, thereby indicating an absence of significant cation exchange within the carbonate brine system.

5. Conclusions

The brine of Na-Cl type in Cambrian carbonate-dominated rocks in the northeastern Chongqing region of Southwestern China is potentially sourced from interstitial fluids present within formations abundant in halite. The brine exhibited an average TDS value of 242 ± 11 g/L. It is noteworthy that the presence of potassium, lithium, and bromine in this brine holds significant potential for industrial mining.

The Cl^-/Br^- ratio indicates that the studied brine underwent moderate seawater evaporation, occurring between the saturation levels of gypsum and halite, accompanied by some degree of halite dissolution. Upon standardization with respect to the chlorinity of modern seawater, the concentrations of Ca^{2+}, Li^+, K^+, Sr^{2+}, and Na^+ in the studied brine were observed to be elevated compared to those in evaporated modern seawater; conversely, the concentrations of Mg^{2+}, Br^-, $HCO_3{}^-$, and $SO_4{}^{2-}$ were notably lower. These anomalous patterns observed in ion concentrations are attributed to various water–rock interactions, including the dolomitization process, combination of halite dissolution and upwelling of lithium- and potassium-bearing groundwater, calcium sulfate precipitation, biological sulfate reduction (BSR), and the common ion effect within the brine. This brine underwent compositional evolution through its interactions with minerals in the surrounding rocks, ultimately resulting in its current chemical composition.

While this study has largely elucidated the sources of the main chemical components in the studied brine, uncertainties remain that necessitate additional isotopic data for validation. Furthermore, both the origin of the water and the chemical components in brine are critically important. Further investigation is warranted to ascertain the specific origins of brine water.

Supplementary Materials: The following supporting information can be downloaded at: https://www.mdpi.com/article/10.3390/w16192859/s1, Figure S1: Trend in anion and cation concentrations, maintaining a relatively stable state over time; Figure S2: Giggenbach triangle plot indicates that the brine was saturated; Table S1: Desulfurization coefficient.

Author Contributions: Conceptualization, Z.-l.Z., K.Z., B.-c.Z. and P.-h.Y.; Data curation, L.Z. and P.-h.Y.; Funding acquisition, Z.-l.Z.; Investigation, Z.-l.Z., B.X., C.-m.W., L.Z. and P.-h.Y.; Methodology, Z.-l.Z. and P.-h.Y.; Project administration, Z.-l.Z. and P.-h.Y.; Resources, Z.-l.Z. and P.-h.Y.; Software, L.Z. and P.-h.Y.; Supervision, P.-h.Y.; Validation and visualization, L.Z. and P.-h.Y.; Writing—original draft, Z.-l.Z., L.Z. and P.-h.Y.; Writing—review and editing, Z.-l.Z., L.Z. and P.-h.Y. All authors have read and agreed to the published version of the manuscript.

Funding: This research was funded by the Chongqing Technology Innovation and Application Development Project, Science and Technology Program from Chongqing Municipal Bureau of Planning and Natural Resources (under grant number: [2023]175-4), and Wuxi County.

Data Availability Statement: Data is contained within the article or Supplementary Material.

Acknowledgments: We express our gratitude to Tao Wang and Jie Feng for their sampling work in the field. We are also deeply appreciative of the valuable and constructive suggestions offered by the four anonymous reviewers, as well as Assistant Editors Keely Zhang and Elma Shi.

Conflicts of Interest: The authors declare no conflicts of interest.

References

1. Person, M.; McIntosh, J.; Kim, J.-H.; Noyes, C.; Bailey, L.; Lingrey, S.; Krantz, R.; Lucero, D.; Reiners, P.; Ferguson, G. Hydrologic windows into the crystalline basement and their controls on groundwater flow patterns across the Paradox Basin, western USA. *Geol. Soc. Am. Bull.* **2024**, *136*, 3156–3168. [CrossRef]
2. Ngombe, O.G.; Walter, J.; Chesnaux, R.; Molson, J. Application of hierarchical cluster analysis and principal component analysis to identify compositional trends of brine in crystalline basements and sedimentary basins. *Appl. Geochem.* **2024**, *169*, 106030. [CrossRef]
3. Marza, M.; Ferguson, G.; Thorson, J.; Barton, I.; Kim, J.-H.; Ma, L.; McIntosh, J. Geological controls on lithium production from basinal brines across North America. *J. Geochem. Explor.* **2024**, *257*, 107383. [CrossRef]
4. Yu, X.C.; Wang, C.L.; Huang, H.; Yan, K. Origin of lithium in oilfield brines in continental petroliferous basin: Insights from Li and Sr isotopes in the Jianghan Basin, central China. *Mar. Pet. Geol.* **2024**, *160*, 106576. [CrossRef]

5. Yoshimura, S. Controls on the Salinity of Sedimentary Basinal Fluids Under Constant Chemogravitational Potential Conditions. *Geochem. Geophys. Geosyst.* **2023**, *24*, e2022GC010628. [CrossRef]
6. Hanor, J.S. *Origin of Saline Fluids in Sedimentary Basins*; Special Publication; The Geological Society of London: London, UK, 1994.
7. Johnson, K.S. Evaporite-karst problems and studies in the USA. *Environ. Geol.* **2008**, *53*, 937–943. [CrossRef]
8. Michael, K.; Machel, H.G.; Bachu, S. New insights into the origin and migration of brines in deep Devonian aquifers, Alberta, Canada. *J. Geochem. Explor.* **2003**, *80*, 193–219. [CrossRef]
9. Ferguson, G.; McIntosh, J.C.; Grasby, S.E.; Hendry, M.J.; Jasechko, S.; Lindsay, M.B.J.; Luijendijk, E. The Persistence of Brines in Sedimentary Basins. *Geophys. Res. Lett.* **2018**, *45*, 4851–4858. [CrossRef]
10. Carreira, P.M.; Marques, J.M.; Nunes, D. Source of groundwater salinity in coastline aquifers based on environmental isotopes (Portugal): Natural vs. human interference. A review and reinterpretation. *Appl. Geochem.* **2014**, *41*, 163–175. [CrossRef]
11. Labotka, D.M.; Panno, S.V.; Locke, R.A.; Freiburg, J.T. Isotopic and geochemical characterization of fossil brines of the Cambrian Mt. Simon Sandstone and Ironton-Galesville Formation from the Illinois Basin, USA. *Geochim. Cosmochim. Acta* **2015**, *165*, 342–360. [CrossRef]
12. Kazemihokmabad, P.; Khamehchi, E.; Kalatehno, J.M.; Ebadi, R. A comparative study of brine solutions as completion fluids for oil and gas fields. *Sci. Rep.* **2024**, *14*, 12628. [CrossRef] [PubMed]
13. Bute, S.I.; Zhou, J.-X.; Luo, K.; Girei, M.B.; Peter, R.T. Pb-Zn-Ba deposits in the Nigerian Benue Trough: A synthesis on deposits classification and genetic model. *Ore Geol. Rev.* **2024**, *166*, 105947. [CrossRef]
14. Stueber, A.M.; Walter, L.M. Origin and chemical evolution of formation waters from Silurian-Devonian strata in the Illinois Basin, USA. *Geochim. Cosmochim. Acta* **1991**, *55*, 309–325. [CrossRef]
15. Billings, G.K.; Hitchon, B.; Shaw, D. Geochemistry and origin of formation waters in the Western Canada Sedimentary. *Chem. Geol.* **1969**, *4*, 211–223. [CrossRef]
16. Graf, D.L. Chemical osmosis, reverse chemical osmosis, and the origin of subsurface brines. *Geochim. Cosmochim. Acta* **1982**, *46*, 1431–1448. [CrossRef]
17. Gianfriddo, C.; Bull, S. Brine reflux as a possible first order control on the alkali geochemistry of baseline sedimentary rocks in the Proterozoic North Australian Zinc Belt. *Precambrian Res.* **2023**, *390*, 107044. [CrossRef]
18. Dugamin, E.J.; Cathelineau, M.; Boiron, M.-C.; Richard, A.; Despinois, F. Lithium enrichment processes in sedimentary formation waters. *Chem. Geol.* **2023**, *635*, 121626. [CrossRef]
19. Warr, O.; Giunta, T.; Onstott, T.C.; Kieft, T.L.; Harris, R.L.; Nisson, D.M.; Lollar, B.S. The role of low-temperature ^{18}O exchange in the isotopic evolution of deep subsurface fluids. *Chem. Geol.* **2021**, *561*, 120027. [CrossRef]
20. Engle, M.A.; Reyes, F.R.; Varonka, M.S.; Orem, W.H.; Ma, L.; Ianno, A.J.; Schell, T.M.; Xu, P.; Carroll, K.C. Geochemistry of formation waters from the Wolfcamp and "Cline" shales: Insights into brine origin, reservoir connectivity, and fluid flow in the Permian Basin, USA. *Chem. Geol.* **2016**, *425*, 76–92. [CrossRef]
21. Saleh, A.; Gad, A.; Ahmed, A.; Arman, H.; Farhat, H.I. Groundwater hydrochemical characteristics and water quality in Egypt's central eastern desert. *Water* **2023**, *15*, 971. [CrossRef]
22. Carpenter, A.B. Origin And Chemical Evolution Of Brines In Sedimentary Basins. In Proceedings of the SPE Annual Fall Technical Conference and Exhibition, Houston, TX, USA, 1–3 October 1978.
23. Mccaffrey, M.A.; Lazar, B.; Holland, H.D. The Evaporation Path of Seawater and the Coprecipitation of Br^- and K^+ with Halite. *J. Sediment. Petrol.* **1987**, *57*, 928–937. [PubMed]
24. Freeman, J.T. The use of bromide and chloride mass ratios to differentiate salt-dissolution and formation brines in shallow groundwaters of the Western Canadian Sedimentary Basin. *Hydrogeol. J.* **2007**, *15*, 1377–1385. [CrossRef]
25. Davisson, M.L.; Criss, R.E. Na-Ca-Cl relations in basinal fluids. *Geochim. Cosmochim. Acta* **1996**, *60*, 2743–2752. [CrossRef]
26. Mirnejad, H.; Sisakht, V.; Mohammadzadeh, H.; Amini, A.H.; Rostron, B.J.; Haghparast, G. Major, minor element chemistry and oxygen and hydrogen isotopic compositions of Marun oil-field brines, SW Iran: Source history and economic potential. *Geol. J.* **2011**, *46*, 1–9. [CrossRef]
27. Darvari, R.; Nicot, J.P.; Scanlon, B.R.; Kyle, J.R.; Elliott, B.A.; Uhlman, K. Controls on lithium content of oilfield waters in Texas and neighboring states (USA). *J. Geochem. Explor.* **2024**, *257*, 107363. [CrossRef]
28. Yan, K.; Wang, C.L.; Chen, R.Y.; Liu, C.L.; Wang, J.Y.; Yu, X.C.; Shen, L.J.; Li, R.Q.; Zhou, Y.; Zhou, Q. Origin and evolution of deep lithium-rich brines in the southwest Jianghan Basin, central China: Evidence from hydrochemistry and stable isotopes. *J. Hydrol.* **2023**, *626*, 130163. [CrossRef]
29. Hu, G.; Teng, J.; Ruan, X.; Wang, Q.; Yan, Y.; Wang, P.; Xiong, S. Magnetic anomaly characteristics and crystalline basement variation of the Qinling orogenic belt and its adjacent areas. *Chin. J. Geophys.* **2014**, *57*, 556–571. (In Chinese with English Abstract)
30. Wang, S.; Zheng, M. Cambrian salt-forming environment in northeastern Sichuan basin and Its significance for finding potash. *Sci. Technol. Rev.* **2014**. *32*, 41–49, (In Chinese with English Abstract)
31. Zhang, J.; Yang, P.; Groves, C.; Luo, X.; Wang, Y. Influence of geological structure on the physicochemical properties and occurrence of middle-deep groundwater in Chongqing, Southwest China. *J. Hydrol.* **2022**, *610*, 127782. [CrossRef]
32. Yang, P.; Cheng, Q.; Xie, S.; Wang, J.; Chang, L.; Yu, Q.; Zhan, Z.; Chen, F. Hydrogeochemistry and geothermometry of deep thermal water in the carbonate formation in the main urban area of Chongqing, China. *J. Hydrol.* **2017**, *549*, 50–61. [CrossRef]
33. Piper, M. A graphic procedure in the geochemical interpretation of water-analyses. *Trans. Am. Geophys. Union* **1944**, *25*, 914–928.

34. Kazakis, N.; Matiatos, L.; Ntona, M.M.; Bannenberg, M.; Kalaitzidou, K.; Kaprara, E.; Mitrakas, M.; Loannidou, A.; Vargemezis, G.; Voudouris, K. Origin, implications and management strategies for nitrate pollution in surface and ground waters of Anthemountas basin based on a δ^{15}N-NO_3^- and δ^{18}O-NO_3^- isotope approach. *Sci. Total Environ.* **2020**, *724*, 138211. [CrossRef] [PubMed]
35. Wu, J.H.; Zhou, H.; He, S.; Zhang, Y.X. Comprehensive understanding of groundwater quality for domestic and agricultural purposes in terms of health risks in a coal mine area of the Ordos basin, north of the Chinese Loess Plateau. *Environ. Earth Sci.* **2019**, *78*, 446. [CrossRef]
36. Chenaker, H.; Houha, B.; Vincent, V. Hydrogeochemistry and geothermometry of thermal water from northeastern Algeria. *Geothermics* **2018**, *75*, 137–145. [CrossRef]
37. Liu, F.; Song, X.; Yang, L.; Zhang, Y.; Han, D.; Ma, Y.; Bu, H. Identifying the origin and geochemical evolution of groundwater using hydrochemistry and stable isotopes in the Subei Lake basin, Ordos energy base, Northwestern China. *Hydrol. Earth Syst. Sci.* **2015**, *19*, 551–565. [CrossRef]
38. Gibbs, R.J. Mechanisms Controlling World Water Chemistry. *Science* **1970**, *170*, 1088–1090. [CrossRef]
39. Marandi, A.; Shand, P. Groundwater chemistry and the Gibbs Diagram. *Appl. Geochem.* **2018**, *97*, 209–212. [CrossRef]
40. Smida, H.; Tarki, M.; Dassi, L. Groundwater quality and mineralization process in the Braga shallow aquifer, Central Tunisia: An overview. *Carbonates Evaporites* **2022**, *37*, 28. [CrossRef]
41. Muhammad, S.; Ullah, I. Spatial and seasonal variation of water quality indices in Gomal Zam Dam and its tributaries of south Waziristan District, Pakistan. *Environ. Sci. Pollut. Res.* **2022**, *29*, 29141–29151. [CrossRef]
42. Ez-zaouy, Y.; Bouchaou, L.; Saad, A.; Hssaisoune, M.; Brouziyne, Y.; Dhiba, D.; Chehbouni, A. Morocco's coastal aquifers: Recent observations, evolution and perspectives towards sustainability. *Environ. Pollut.* **2022**, *293*, 118498. [CrossRef]
43. Shen, B.B.; Wu, J.L.; Zhan, S.; Jin, M.; Saparov, A.S.; Abuduwaili, J. Spatial variations and controls on the hydrochemistry of surface waters across the Ili-Balkhash Basin, arid Central Asia. *J. Hydrol.* **2021**, *600*, 126565. [CrossRef]
44. Chen, Y. Sequence of salt separation and regularity of some trace elements distribution during isothermal evaporation (25 °C) of the Huanghai Sea water. *Acta Geol. Sin.* **1983**, 379–390. (In Chinese with English Abstract)
45. Gavrieli, I.; Stein, M. On the origin and fate of the brines in the Dead Sea basin. In *New Frontiers in Dead Sea Pale-Oenvironmental Research*; Enzel, Y., Agnon, A., Stein, M., Eds.; Geological Society of America Special Paper 401; Geological Society of America: Boulder, CO, USA, 2006; pp. 183–194.
46. Parnell, J.; Armstrong, J.G.T. Surface expression of Late Caledonian magmatic lithium concentration, in the Rhynie Chert, UK. *Geochem. Explor. Environ. Anal.* **2023**, *23*, geochem2023-028. [CrossRef]
47. You, C.F.; Chan, L.H. Precise determination of lithium isotopic composition in low concentration natural samples. *Geochim. Cosmochim. Acta* **1996**, *60*, 909–915. [CrossRef]
48. Herrera, C.; Godfrey, L.; Urrutia, J.; Custodio, E.; Gamboa, C.; Jódar, J.; Lam, E.; Fuentes, J. Origin of old saline groundwater in the deep coastal formations of the Atacama Desert region: Consideration of lithium, boron, strontium and uranium isotopes contents. *J. Hydrol.* **2023**, *624*, 129919. [CrossRef]
49. Yu, F.; Yu, Y.; Wang, D.; Gao, J.; Wang, C.; Guo, W. Application of Li isotope in geothermal fluid-rock interaction: A case study of modern Li-rich geothermal water in western Sichuan. *Acta Petrol. Sin.* **2022**, *38*, 472–482. (In Chinese with English Abstract)
50. Yang, N.; Su, C.L.; Liu, W.B.; Zhao, L. Occurrences and mechanisms of strontium-rich groundwater in Xinglong County, northern China: Insight from hydrogeological and hydrogeochemical evidence. *Hydrogeol. J.* **2022**, *30*, 2043–2057. [CrossRef]
51. Trudinger, P.A.; Chambers, L.A.; Smith, J.W. Low-temperature sulphate reduction: Biological versus abiological. *Can. J. Earth Sci.* **1985**, *22*, 1910–1918. [CrossRef]
52. Yang, P.H.; Yuan, D.X.; Ye, X.C.; Xie, S.Y.; Chen, X.B.; Liu, Z.Q. Sources and migration path of chemical compositions in a karst groundwater system during rainfall events. *Chin. Sci. Bull.* **2013**, *58*, 2488–2496. [CrossRef]
53. Yang, P.H.; Luo, D.; Hong, A.H.; Ham, B.; Xie, S.Y.; Ming, X.X.; Wang, Z.X.; Pang, Z.H. Hydrogeochemistry and geothermometry of the carbonate-evaporite aquifers controlled by deep-seated faults using major ions and environmental isotopes. *J. Hydrol.* **2019**, *579*, 124116. [CrossRef]
54. Blasco, M.; Auque, L.F.; Gimeno, M.J. Geochemical evolution of thermal waters in carbonate—Evaporitic systems: The triggering effect of halite dissolution in the dedolomitisation and albitisation processes. *J. Hydrol.* **2019**, *570*, 623–636. [CrossRef]
55. Gil-Marquez, J.M.; Barbera, J.A.; Andreo, B.; Mudarra, M. Hydrological and geochemical processes constraining groundwater salinity in wetland areas related to evaporitic (karst) systems. A case study from Southern Spain. *J. Hydrol.* **2017**, *544*, 538–554. [CrossRef]